Comparison of Objectives in Multi-Objective Optimization of Ultrasonic Positioning Anchor Placement

Sebastian Haigh, *Member, IEEE,* Janusz Kulon, *Senior Member, IEEE,* Adam Partlow, and Colin Gibson

***Abstract*—The position of anchors in an ultrasonic positioning system has a significant impact on the performance of that system. This impact on performance can be in the form of positioning error, how large of a space the system can cover, and then number of anchors required. A comparison of three different performance metrics for anchor position optimization in ultrasonic localization systems is presented. These metrics are geometric dilution of precision (GDOP), weighted GDOP (WGDOP), and simulated localization error (SLE). Each of these performance metrics is used as an objective in a multi-objective genetic algorithm. The optimal solutions found by the genetic algorithm were processed by a simulation that used a simulated received time series to localize the target position allowing a direct comparison of the three performance metrics. While the performance difference between all three metrics was small, it was found that solutions generated using WGDOP as a metric of performance outperformed those generated using the GDOP and the SLE objectives.**

***Index Terms*—Genetic algorithms, Pareto optimization, acoustic local positioning, geometrical dilution of precision, accuracy**

I. Introduction

ULTRASONIC positioning systems (UPSs) consist of several nodes, with each node equipped with appropriate transducers that allow either the transmission or reception of ultrasonic signals. Some of these nodes are in known positions, termed anchor nodes, while other nodes are in unknown positions, termed target nodes. The goal of the positioning system is to find the position of the target nodes. The system gains information by the passing of signals between the nodes, and then combines this with information already known, i.e., the anchor node positions, to estimate the target node position. A common method employed for extracting useful information from signal passing is to measure the time of flight (TOF) of the acoustic signals as they propagate between nodes. From the TOF, the distance between the nodes can be estimated, with some error $\varepsilon \sim \mathcal{N}(0, \sigma^2)$, where $\mathcal{N}(\mu, \sigma^2)$ is a normal distribution with mean μ and variance σ^2. The distance observed between the kth anchor and a target is denoted d_k. The pseudo-range d_k is related to the known position of the anchor $\boldsymbol{\rho}_k = [x_k, y_k, z_k]^T$, the unknown position of the target $\mathbf{p} = [x, y, z]^T$, and the error ε as follows

$$d_k = \|\mathbf{p} - \boldsymbol{\rho}_k\| + \varepsilon_k. \tag{1}$$

The estimation of $\mathbf{p}$ corresponds geometrically to estimating the point of intersection of N spheres where each of the spheres have centers located at $\boldsymbol{\rho}_1, \boldsymbol{\rho}_2, \ldots, \boldsymbol{\rho}_N$, each sphere has radius $d_1, d_2, \ldots, d_N$, and the point of intersection is $\mathbf{p}$. Many estimators exist for solving such a system, for example least square estimators can be used where the ε_k are independent and identically distributed (i.i.d.) and Gaussian.

Whereas the i.i.d. Gaussian assumption on the noise term makes deriving a suitable estimator simpler, it is an oversimplification in many cases. The ε_k will not be i.i.d. as the signals from each anchor will not be identically attenuated due to differences in the distance travelled. Differences in attenuation result in a different SNR for each signal and a different error variance for each d_k. Furthermore, the error distribution will not be exactly Gaussian due to non-Gaussian noise sources such as multipath interference, where acoustic signals have reflected from surfaces in the environment, and constructive and destructive interference, where signals arrive at the microphone at the same time. Such interference has been documented to cause large errors in acoustic positioning systems [1].

The physical layout of the anchor nodes impacts the performance of the system in several ways. Firstly, the anchor position affects the ε_k through signal attenuation by altering the distance that must be traveled to a given target. Secondly, the anchor positions impact the number of anchors that can be seen by a target in any given position. This effect on the available anchor-target line of sight paths will impact the performance of the system when obstructions are introduced. Finally, the geometric dilution of precision (GDOP) is dependent on the distribution of the anchors and can have a substantial effect on the accuracy of localization. The GDOP is a single dimensionless number that captures how the relative positions of the anchor nodes $\boldsymbol{\rho}_1, \ldots, \boldsymbol{\rho}_N$ affect the propagation of error from the range measurements d_k to the estimate of $\mathbf{p}$ [2].

The optimization of anchor node positions has been extensively explored in the literature. However, much of the literature is focused upon node placement in wireless sensor

This work was supported by: a) the University of South Wales through the CES Research Investment Scheme Grant (Ref. 100954.1125), b) the Higher Education Investment and Recovery Fund (Ref 102677.1122) and c) the Cardiff and Vale University Health Board's Rehabilitation Engineering Unit (EFAS 22395).

S. Haigh and J. Kulon are with the Faculty of Computing, Engineering and Science, University of South Wales, Pontypridd CF37 1DL, U.K. (e-mail: sebastian.haigh@southwales.ac.uk; j.kulon@southwales.ac.uk).

A. Partlow and C. Gibson are with the Rehabilitation Engineering Unit, Artificial Limb and Appliance Service, Cardiff and Vale University Health Board, Cardiff CF37 5TF, U.K.

networks (WSNs), where positioning accuracy is often a minor concern [3]. In [4], it was noted that the GDOP has not been deeply investigated for indoor ultrasonic positioning systems and [4] introduced a method of anchor position optimization for a UPS, based on a Monte-Carlo simulation method, using GDOP as metric of performance. Similar GDOP optimizations have been investigated for other forms of positioning systems such as in [5]. In [6], GDOP is employed along with the eigenvalues of the inverse FIM, which take into account the shape of the error ellipsoid. While finding success in optimizing the positions with respect to their chosen objective functions, neither [5] nor [6] consider other factors that the anchor positions impose upon the precision of the system such as transducer directionality and signal attenuation.

Weighted GDOP (WGDOP) has been suggested as an alternative to GDOP [7]. As mentioned above, the ε_k in (1) are assumed to be i.i.d. This assumption is extended to the derivation of GDOP. However, this is rarely the case in practice, and the variance of Gaussian noise varies between the different signals. In acoustic positioning systems, the main contributing factors to variance differences are 1) signal attenuation due to distance from the signal source to the target and 2) attenuation of transmitted and received signals due to the directivity of the transducers.

Whereas minimizing measurement error is not always a primary concern for WSNs, maximizing target node coverage has seen significant interest. Target node coverage refers to ensuring that the target has a line of sight to a minimum number of anchors regardless of its position in space. In [8] it is noted that finding the minimum number of anchors to cover a target is similar to the art gallery problem described in [9], however, in localization, multiple anchors must have a LOS path to the target for position estimation to be possible. A κ-coverage criteria can be introduced to manage the minimum LOS anchor problem such as in [8], where a target must have a line of sight to at least κ anchors to be considered covered, and greater values of κ result in greater system redundancy.

In [10] and [5], GDOP is combined into a single objective function with quantification of singular areas (SA) and non-coverage areas (NC). SA are areas where the only anchors available to target are arranged in a straight line and NC are areas where there are not enough anchors available to the target for position estimation. In [10], a diversified local search (DLS) is employed as an alternative to a genetic algorithm (GA) approach. DLS is a heuristic search approach which is divided into two phases: intensification and diversification. The intensification phase takes the currently highest performing anchor arrangement and moves anchors by small fixed increments and assesses their performance in each of these positions. When a better solution is found for an anchor, the search is stopped, and the new, superior anchor position adopted. Once the local neighborhood has been exhaustively searched, the resulting anchor positions are considered locally optimal, and the algorithm moves to the diversification phase, which attempts to break out of the local optimum and move the search towards a global optimum.

The DLS searches faster than the GA to which it was compared and achieved superior performance in some cases, however, there are factors that make it unsuitable for the current work. Firstly, there is a limited amount of evidence in support of its use and performance and that evidence deals only with 2D localization scenarios. The goal of this paper is to present a comparison of performance objectives that will be useful to a wide range of researchers. DLS has not been used as widely as GAs and therefore the results would be more widely accessible if a more widely used technique was used to implement the optimization. Additionally, DLS does not have the automatic support for a variable number of anchors that is supported by some GAs. DLS technique would require the optimization to be run separately for each number of anchors and then the performance of these solutions would have to be analyzed separately on the results of the individual optimizations.

An evolutionary strategy was applied in [6] using a non-dominated sorting genetic algorithm (NSGA), for use in optimizing the positions of sensors in a range difference of arrival (RDOA) localization system. The approach in [6] uses the CRLB as a method of determining the performance of the system by calculating the Fisher information matrix for RDOA localization. This objective is combined with target coverage and the number of sensors to form a multi-objective optimization problem. A different evolutionary strategy is applied in [11], with a method based upon NeuroEvolution of Augmenting Topologies (NEAT) [12], [13]. The method developed in [11], termed Flexible Algorithm for Sensor Placement (FLEX), combined the complexification techniques of NEAT with the Pareto dominance of NSGA, and a similar approach will be adopted in this paper as it combines multi-objective GA optimization, with flexible-length genotypes.

In this paper, a multi-objective genetic algorithm is developed using a simulation of the received time series for assessment of possible solutions. The genetic algorithm approach was chosen as it offers good optimization performance when using a complex simulation as an assessment of solution fitness. The effect of the sensor placement on UPSs can not be reduced to a simple loss function based on GDOP, as has been applied in previous work. Other factors contribute to the performance beyond the presence of Gaussian noise such as signals arriving outside their assigned time slots in time division multiple access (TDMA) schemes.

This paper claims the following novel contributions:

- Application of WGDOP to anchor position optimization in 3D acoustic localization systems, where information about acoustic signal attenuation is combined with the GDOP by introducing an exponential precision model.
- A comparison of three different objective functions that can be used for optimizing anchor positions in acoustic localization systems (GDOP, WGDOP, and simulated localization error (SLE)).

Section II describes how the objectives for the multi-objective optimization were calculated, with specific attenuation applied the computation of the WGDOP and SLE objectives. Section III provides an overview of the genetic algorithm that will be used to perform the optimization. The simulation created to assess anchor positions is presented in Section IV. Results and discussion are presented in Section V.

II. Objective Simulation

The scenario considered for this optimization is a room with a 2000 mm x 3000 mm floorplan and a height of 2000 mm and with four rectangular columns extending from the floor to the ceiling. The floorplan of the simulated room is shown in Fig. 1. Test points for the target position were evenly spaced within this volume at intervals of 250 mm in all three axes. Anchors could be placed upon the four walls of the room and the ceiling. This environment creates a challenging situation for a UPS. In such a complex environment, the problem of finding high performing anchor layouts is challenging and necessitates optimization. This environment is, therefore, similar to where this optimization method may be employed in practice.

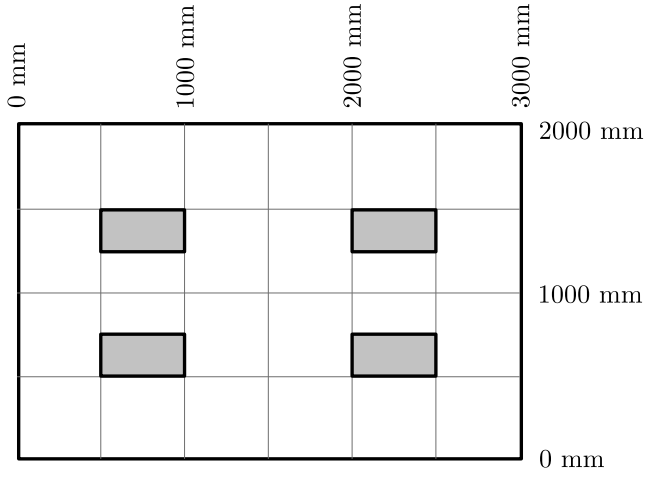

Figure 1. The environment in which the simulations were conducted. Positions of obstructions are depicted as grey rectangles.

In any given optimization, the algorithm assessed the fitness of a set of anchors against three objectives:

1) the number of anchors,
2) the percentage of target positions covered by at least four anchors, and
3) a performance metric related to localization error.

Three different performance metrics were utilized (GDOP, WGDOP, and SLE) to create three distinct multi-objective optimizations.

The first objective, i.e., the number of anchors, can be found simply by counting the number of anchors in any given set. The second, i.e., target coverage, requires checking the LOS paths between anchors and target using a line-triangle intersection algorithm. Line segments extended from the anchor to the target position, and each obstruction was modelled by a triangular mesh.

In all three performance metrics, the metric is calculated for each target position that met the target coverage condition of a LOS path to at least four anchors. The final objective score was then calculated as the mean average of these individual metrics over all target positions. GDOP is the simplest performance metric and can be computed as

$$\text{GDOP} = \sqrt{\text{Tr}((\mathbf{G}^T\mathbf{G})^{-1})}. \tag{2}$$

The matrix $\mathbf{G}$ is a function of only the target and anchor geometry. For pseudo-range measurements, this matrix is the Jacobian of the error-free version of (1) [14]

$$\mathbf{G}_{kj} = \frac{\partial d_k}{\partial \mathbf{p}_j} = \frac{\mathbf{p}_j - \boldsymbol{\rho}_{kj}}{\|\mathbf{p} - \boldsymbol{\rho}_k\|}, \tag{3}$$

where d_k refers to the kth range measurement, $\mathbf{p}_j$ refers to the jth component of the target position vector and $\boldsymbol{\rho}_{kj}$ is the jth component of the position vector of the kth anchor. WGDOP is defined similarly to GDOP, but with the introduction of a weight matrix $\mathbf{W}$

$$\text{WGDOP} = \sqrt{\text{Tr}\left((\mathbf{G}^T\mathbf{W}\mathbf{G})^{-1}\right)}, \tag{4}$$

where $\mathbf{W}$ is defined as

$$\mathbf{W} = \begin{bmatrix} 1/\sigma_1^2 & 0 & \cdots & 0 \\ 0 & 1/\sigma_2^2 & \cdots & 0 \\ 0 & 0 & \ddots & \vdots \\ 0 & 0 & \cdots & 1/\sigma_n^2 \end{bmatrix}, \tag{5}$$

and the $\sigma_1^2, \ldots, \sigma_n^2$ are the variances of signals from anchors $1, \ldots, n$.

The SLE is a simplified simulation of the expected localization error for a given anchor layout. Unlike the dimensionless quantities of GDOP and WGDOP, the SLE objective returns an error in mm. The simulation of localization error worked by estimating the range measurement error from each anchor and adding these errors to the known distance between an anchor and target to create simulated noisy measurements. These noisy measurements were then used to estimate the target position using a Levenburg Marquardt (LM) least squares estimator. The SLE for a single target position was calculated as the Euclidean distance between the estimated and known position of the target.

Both WGDOP and SLE require further simulation to calculate than GDOP. The weights in WGDOP are individually assigned based on the expected error contribution from each anchor. The larger the error from an anchor is expected to be, the higher the weight. Similarly, for SLE, the range measurement error must be calculated individually for each anchor. Both approaches require modelling of the attenuation of acoustic signals (detailed in section II-A), which is the same for both WGDOP and SLE objectives. Also required is modelling of affect of attenuation on error variance of range measurements, and, for SLE, the generation of noisy range measurements from this error variance (as detailed in section II-B). Finally, for the SLE objective, the 3D position must be estimated as described in section II-C.

A. Attenuation Modelling

The attenuation of acoustic signals is a significant factor affecting the performance of range estimation with ultrasound. This attenuation has two contributing factors: the distance traveled by the acoustic signal and the transducer directionality. Previous research [15], [16] has shown that - while the accuracy of range estimation certainly decreases with distance - the effect of directionality is especially pronounced. Acoustic

transmitters do not output acoustic signals with equal sound pressure level in all directions of the signals' spherical propagation pattern. Due to the significance of these two factors on both range measurement and 3-D position estimation error, they both had to be included in the simulated model. Attenuation due to distance was modeled as a geometric spreading loss [17] of an acoustic wave propagating spherically from a point source. The attenuation due to transducer directionality was modeled with polynomial models derived from the datasheet the Murata MA40SAS ultrasonic transducer.

As above, the distance between the kth anchor and the target is denoted d_k. The angle of transmission from the kth anchor is denoted θ_k and is the angle between the anchor-to-target LOS path and the transducers direction of maximum directivity (DMD). For the transducers modeled in this work, the DMD is a vector colinear to the transducers cylindrical axis. Attenuation is denoted by a with attenuation due to distance being denoted a_d, attenuation due to the angle θ being denoted a_θ. The total attenuation, taking both distance and directivity into account, is denoted a_T.

According to the datasheet, the Murata MA40SAS has an output signal strength of 120 dB sound pressure level (dB SPL) at 0°, with 0 dB reference of $2\times10^{-5}\,\text{Pa}/10\,\text{V}_{\text{RMS}}$ at 30 cm. This strength decreases as the angle from the transducers central axis increases. The magnitude of the attenuation with respect to angle can be seen in Fig. 2. These values were recorded experimentally, by the manufacturer, at a distance of 0.3 m from the transducer. Thus, a_θ will always refer to an attenuation at a distance of 0.3 m from the source transmitter.

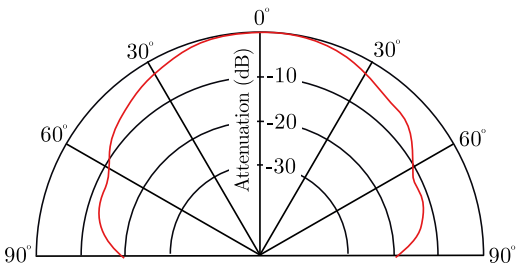

Figure 2. Directivity of Murata MA40SAS Ultrasonic Transmitter.

To model the attenuation due to distance, geometric spreading loss was used. According to [17], the geometric spreading loss (a_s) for an acoustic signal propagating spherically from a point source is expressed, in dB, as

$$a_s = 20\log_{10}\left(\frac{r_2}{r_1}\right)\text{dB}. \tag{6}$$

The expression in (6) models the attenuation that the signal experiences as it travels between a distance r_1 from the source to a distance r_2 from the source, i.e., as its wave front expands from a sphere with radius r_1 to a sphere with radius r_2. Since, $20\log_{10}(2)\approx 6\,\text{dB}$, and an attenuation of $-6\,\text{dB}$ is equivalent to reducing the amplitude by half, this model will half the amplitude of the acoustic wave every time the propagation distance doubles. For the simulation, the radius of the larger sphere (r_2) was taken to be d_k (the distance between the anchor and target) while the radius of the smaller sphere was taken to be 0.3 m (the distance from the anchor for which the SPL is known from the datasheet). Owing to the design of the simulation d_k will always be greater than 0.3 m. Attenuation due to distance is, therefore given by

$$a_d(d) = -20\log_{10}\left(\frac{d}{0.3}\right). \tag{7}$$

In [18], the MATLAB polyfit function was used to fit a 3rd order polynomial to seven samples of the directivity data from the Murata MA40SAR transducer datasheet. The seven samples were taken between 0° and 90° at intervals of 15°. The same method has been applied here; however, more samples were taken of the directivity data, and a 2nd, rather than 3rd, order polynomial was fit to this data. The sampled data, and the 2nd order polynomial, are shown in Fig. 3. The 2nd order polynomial was chosen as it provided a better fit to the sampled data than a 3rd order polynomial.

The polynomial was of the form

$$a_\theta(\theta_k) = c_1\theta_k^2 + c_2\theta_k + c_3, \quad 0^\circ \le \theta_k \le 90^\circ, \tag{8}$$

where θ_k is the angle, in degrees, between the DMD of the kth anchor and LOS path from that anchor to the target. The coefficients c_1, c_2, c_3 are as shown in Table I. The datasheet does not provide data for angles greater than 90°. Therefore the model defined by (8) is only valid for non-negative angles less than 90°. For transmission angles greater than 90°, the simulation will consider that anchor and target are not connected by a LOS path. This choice is justified since all simulated anchors are placed with their DMD normal to a wall. Thus the wall will block transmission at any angle greater than 90° from the DMD. The receiver was modelled as perfectly omnidirectional and its sensitivity was neglected.

Equations (7) and (8) are combined to produce the total attenuation, a_T, which is the sum of $a_\theta(\theta_k)$ and $a_d(d_k)$

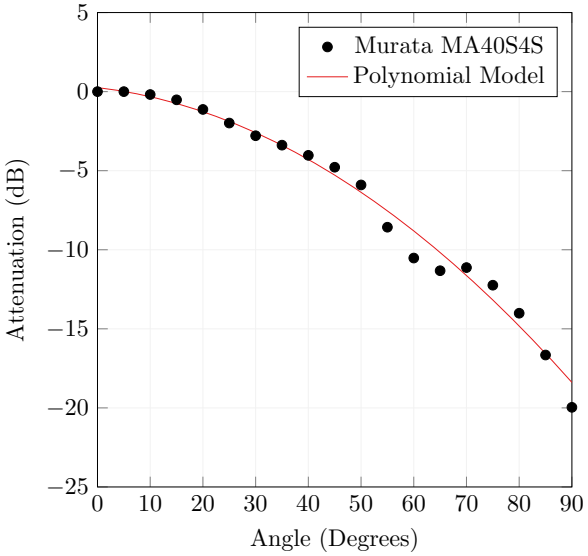

Figure 3. Second order polynomial (red line) fit to samples of the Murata MA40SAS directivity data (black dots) found in the data sheet.

Table I
COEFFICIENTS FOR DIRECTIONALITY POLYNOMIAL MODEL

c_1	c_2	c_3
-0.00187	-0.03889	0.25518

$$a_T(d_k, \theta_k) = a_\theta(\theta_k) + a_d(d_k). \tag{9}$$

B. Variance & Error Modelling

A model of ranging precision against received signal strength in dB SPL was developed from experimental data previously collected as part of the work presented in [16]. The data were processed to obtain the range measurement error and estimated dB SPL of each acoustic pulse arriving at the microphone. These data were aggregated to obtain a histogram of ranging precision given received signal strength. An exponential model of the form $z = Ae^{Bx} + C$ was then fit to the histogram using the LM algorithm, where y is the ranging precision, and x is the received signal strength in dB SPL. The resulting fitted model was:

$$z = 2.4829 \times 10^{-14} e^{0.2618x} + 0.004 \tag{10}$$

The weights for the WGDOP were variances calculated from the precision model, i.e., $1/z$. For the SLE objective, the errors for the range measurements were sampled from a normal distribution with a mean of zero and precision given by z.

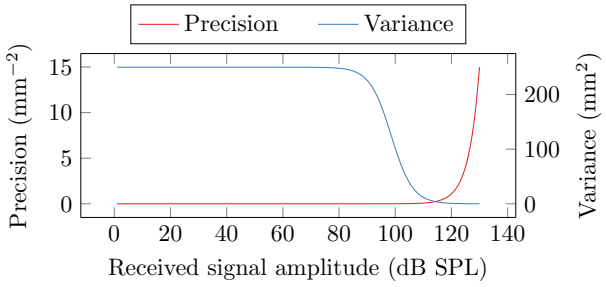

Figure 4. Values of the precision model (17), and its inverse, for received signal amplitudes of 1 to 130 dB SPL. Precision model values are shown in red while those of variance are shown in blue.

C. 3-D Position Estimation

The simulated noisy measurements generated from a normal distribution with precision given by (10) were used estimate the position of the target using a LM least squares estimator. The LM estimator has the following update equation:

$$\mathbf{p}_{i+1} = \mathbf{p}_i - \left(\mathbf{J}^T\mathbf{J} + \lambda \text{Diag}(\mathbf{J}^T\mathbf{J})\right)^{-1} \mathbf{J}^T\mathbf{r}, \tag{11}$$

where $\mathbf{J}$ is the Jacobian matrix of the system of equations in (1), $\mathbf{r}$ is the vector residuals between the simulated noisy measurements and those calculated from the ith iterations estimate of the target position $\mathbf{p}_i$ and (1). The quantity λ is a damping parameter that is initialized at $\lambda = 10,000$ and is increased or decreased depending on convergence.

III. GENETIC ALGORITHM

A GA is a metaheuristic optimization strategy inspired by natural selection. These algorithms apply various mutations, crossover, and selection strategies to a population of possible solutions to a given problem, enabling a broad search of the solution space. The population was a set of anchor configurations, where each member of the population was an N_a-tuple of anchor positions where N_a is the number of anchors in a given solution. The population was defined as a set $\mathcal{P} = \{G_1, G_2, \ldots, G_M\}$, where each of the G_i are genotypes $G_i = (g_1, g_2, \ldots, g_N)$, and each of the g_i is an individual gene, which provides enough information to specify the position of an anchor.

The NEAT algorithm was chosen as the base algorithm for this optimization. The NEAT algorithm is suited to this problem as it allows for a variable genotype size. A variable genotype length is required for this optimization in order to compare solutions with different number of anchors, enabling the number of anchors to be minimized, and finding the highest performance anchor placement for different number of anchors. NEAT enables a variable genotype length by introducing a historical marker for each gene. The historical marker is a global counter that is incremented by one every time a new gene is created. When the gene is created it is assigned the new value of the historical marker, which it will retain for its entire existence. Any offspring of genotypes that receive this gene, will also receive its historical marker. Each historical marker therefore has a single genesis point at which it was created and allows for the tracking of speciation within the algorithm.

The genes were defined as $g_i = (\boldsymbol{\rho}_i, W, H)$, where $\boldsymbol{\rho}_i$ is the position of the anchor, W is an identifier of the wall or surface that the anchor is attached to, and H is the NEAT historical marker for this gene. The wall identifier W is required to determine the direction in which the anchor is pointing. To simplify the problem, it was assumed that each anchor was positioned such that its central axis was normal to the surface on which it was placed. Therefore, the direction vectors were defined as the normal vector to the surface and - since all of the surfaces were flat planes - this vector was equal for every anchor on the same surface.

Two genotypes are considered to have the same species if the compatibility distance δ between them is less than a given threshold. When comparing two genotypes, genes that occur in both genotypes are called matched genes. Genes that are not matching are termed either disjoint or excess. In Fig. 5, genes 1, 2, 3, and 6 are all matched genes, genes 4 and 5 are both disjoint genes as they are not matched but their historical markers are less than that of the greatest matched gene (gene 6). Gene 7 in parent one is an excess gene, this gene has no matched counterpart in parent 2, but its marker number is greater than that of the greatest matched gene. The compatibility distance is defined in [12] as

$$\delta = \frac{c_1 E}{N} + \frac{c_2 D}{N} + c_3 \overline{w} \tag{12}$$

where E is the number of excess genes, D is the number of disjoint genes, and w is the average weight difference of the

matching genes. The original purpose of the NEAT algorithm was for the training of neural networks, where genes would represent connections and weights between artificial neurons. For anchor position optimization, the average weight difference is replaced by the average Euclidean distance between matching genes, where each gene is a 3D anchor position. It is suggested in [12] that for genotypes with less than 20 genes N can be set to 1.

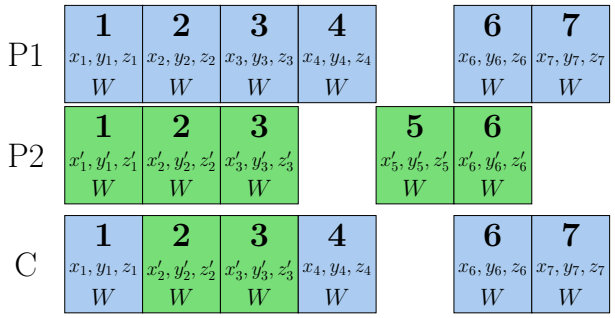

Figure 5. An illustration of matched, disjoint, and excess genes between two parents (P1 and P2) and how this effects the genes that are past to the child (C). Each gene contains a position (x, y, z) and a wall W.

A. Objectives & Non-Dominated Sorting

Three objectives were chosen for this algorithm: target coverage, a localization performance metric (either unit variance GDOP, weighted GDOP or simulated localization error), and number of anchors. Target coverage was calculated as the percentage of target positions that have LOS connection at least four anchors. The localization error was the mean localization error over all of the target positions.

In a multi-objective optimization the goal is to find the Pareto Frontier (PF) which is the set of solutions where the performance of no individual objective can be further improved without degrading performance in another objective. Any solution for which a definitively superior solution exists is called an inferior or dominated solution. All those solutions that are not dominated by any other solution are called non-dominated solutions.

The notation $O_j(G_i)$ represents the score received for the jth objective by the ith genotype. Thus the inequality $O_j(G_i) > O_j(G_k)$ means that the ith genotype received a higher score than the kth solution for the jth objective. However, higher does not universally mean better, since some objectives are required to be minimized. For this reason, the symbol $\succ$ is adopted to mean "better than", and the symbol $\not\prec$ is used to mean "not worse than". Thus we write $O_j(G_i) \succ O_j(G_k)$ to represent that the ith solution performs better than the kth for the jth objective. According to the rules defined in [19], with two solutions (G_1 and G_2) and M objectives ($O_j(\cdot)$ where $j = 1, 2, \ldots, M$) then G_1 can be said to dominate G_2 if the following two statements are true:

$$O_j(G_1) \not\prec O_j(G_2), \ \forall j = 1, 2, \ldots, M, \tag{13}$$

$$O_j(G_1) \succ O_j(G_2), \ \text{for at least one } j = 1, 2, \ldots, M. \tag{14}$$

That is, G_1 must not be worse than G_2 in any of the M objectives and G_1 must be better than G_2 in at least one of those objectives.

The population is sorted by splitting the assessed population into non-dominated fronts. To find a non-dominated front, each genotype in the population is checked against every other genotype using the criteria in (13) and (14). Any genotype fails this test once is marked as dominated. After all of the population has been checked, the genotypes that have not been marked as dominated are separated from the rest of the population forming the 1st non-dominated front. The above process is repeated for the remaining genotypes in the solution until all genotypes have been assigned to a front.

Within each front a final fitness value is calculated for every genotype. Firstly, the sharing distance s_{ij} is between every G_i and G_j in the front using

$$s_{ij} = \sqrt{\sum_{p=1}^{P} \left(\frac{O_p(G_i) - O_p(G_j)}{O_p^{\max} - O_p^{\min}} \right)^2}, \tag{15}$$

where $O_p^{\max}$ is the upper limit of the pth objective and $O_p^{\min}$ the lower limit of the pth objective in this front. These distances were calculated between every member of the each front, and were used to detect close clustering of solutions using the sharing radius σ_s. Over population of a particular niche of the solution space harms the performance of the algorithm. The final fitness score of each solution was degraded to reflect how populated a solution's particular niche was. Punishing population members for clustering close together in the solution space encourages multiple niches to develop and flourish along the PF. To perform this degradation, the distances calculated above are fed into the following sharing function:

$$\mathrm{Sh}(s_{ij}) = \begin{cases} 1 - \left(\dfrac{s_{ij}}{\sigma_s} \right)^2, & s_{ij} \leq \sigma_s \\ 0, & \text{otherwise} \end{cases} \tag{16}$$

where σ_s is the sharing radius. If the jth solution is outside the sharing radius of the ith solution then the result is zero, however if it is inside then the sharing function will return a value between 0 and 1.

Once the sharing function was computed for every jth solution compared to the ith solution, then the degradation factor for the ith solution was calculated:

$$m_i = \sum_{j=1}^{n_k} \mathrm{Sh}(d_{ij}) \tag{17}$$

Finally the overall fitness score f'_i was calculated using:

$$f'_i = \frac{f_k}{m_i} \tag{18}$$

where f_k is a dummy fitness value that can be initialized to some large number. The more solutions that are close together, the larger the value of m_i will be. Thus, the fitness f'_i will be smaller if there are many solutions close to this one and greater if there are few.

B. Breeding

Breeding was conducted using the NEAT breeding strategy, using the compatibility threshold and the concept of matched, disjoint and excess genes. Two genotypes are selected randomly from the same species, as determined by (12). The genes of the two genotypes are lined up as in Fig. 5 and their mutual matched, disjoint, and excess genes are found. The child genotype will inherit matched genes from either parent with equal probability, whereas the child will inherit all disjoint and excess genes from the fitter of the two parents. This process results in more genetic material from fitter solutions being passed into the subsequent generation. As this method uses the final fitness calculated during the non-dominated sorting process, it also preserves the niche size control mechanism from NSGA. Genotypes in more crowded niches will receive a lower overall score, and therefore, less of their genes will be passed on until the size of the niche reduces.

C. Mutations

Three types of mutation were used in this algorithm. These mutations were: add-gene, delete-gene, and change-position. If a genotype is selected for mutation, then one of these four mutations will be applied to that genotype. The mutation that is applied is chosen with uniform probability. The add-gene mutation adds a single gene to a given genotype. When a gene is added, the global value of the historical marker is incremented, and the new marker value is assigned to the added gene. The gene is then randomly assigned a wall in the simulated environment and an anchor position in that wall. Once created, a gene will always keep the same wall. This policy maintains consistency between genotypes of the same species. The delete-gene mutation selects, with uniform probability, one gene from a given genotype and removes it from the genotype.

The change-position mutation moves the gene's anchor to a new position on the gene's assigned wall. This mutation works by generating a random vector in the plane of the wall and adding this vector to the existing position. If the new position is beyond the limits of the wall, then the new randomized position is selected for the gene.

D. Speciation

When the initial population is created, a single new species is also created. Every member of the population is assigned to this single species. The algorithm will create different species in subsequent generations. Each new genotype produced in a generation (either through breeding or mutation) is checked against every surviving member of the previous generation by comparing the species distance between the two genotypes against a threshold. The new genotype is placed into the same species as the first genotype for which the distance is less than the threshold. If the new genotype is outside the threshold for every population member, then a new species is created and assigned to the new genotype. The threshold is dynamic, and its value is updated based on the number of species in the population. The threshold is decreased if the number of species is less than the desired number and increased otherwise, allowing the number of species to be maintained at the desired level.

E. GA Parameter Selection

The population size was set to 150 for every generation. The initial seed contained five anchors. From this seed, the initial 150 population members were created. The wall for each gene in the seed was selected randomly from the available walls in the simulation, and the initial anchor position in each gene was selected as a random position on that wall. The compatibility threshold for NEAT breading was two, and the sharing radius for non-dominated sorting was one. The initial dummy fitness for non-dominated sorting was selected as 10000. This dummy fitness acted as the initial fitness in the first non-dominated front of each generation.The choice of this value is arbitrary and need only be a large value, since the final fitness assigned to each individual is dominated by its proximity to other solutions through (15), (16), (17), and (18), rather than the initial choice of dummy fitness. The initial fitness in all other fronts was calculated by subtracting ten from the previous front's lowest fitness. The mutation rate was selected as 50%, the algorithm is tolerant to high mutation rate due to the protections provided by NEAT speciation. This mutation rate was the probability of a member being selected for mutation. Once selected, the applied mutation was selected from the available four mutation types with uniform probability. A summary of all GA parameters is shown in Table II. The GA was run until there had been no change in the 1st non-dominated front for 50 generations.

IV. Full Time Series Simulation

The abstractness of both GDOP and WGDOP compared to the SLE makes these metrics challenging to compare in practice. One of the objectives of this work was to determine how well each of these individual performance metrics works compared to the others. To directly compare them, the optimum solutions found by each method were further assessed using a more sophisticated simulation, which attempted to model as much of a UPS as possible. The method chosen was to develop a model of the time series of the signal received at the target microphone, which allowed for both Gaussian effects and non-Gaussian effects to be modelled. Non-Gaussian effects of interest to this application include fading due to overlapping received signals, signals arriving in the wrong time slots, and multipath reflections. Simulating this time series had four components, simulation of: 1) the time series of individual signals, 2) signal attenuation, 3) signal propagation delay, and 4) Gaussian interference by the addition of Gaussian noise to the simulated signal. Once the simulator had generated the time series, the range between anchors and targets was measured from that time series, and the 3D position of the target was estimated with an LM estimator.

A. Simulating the Time Series of Individual Signals

The time series of transmitted signals was simulated using an FIR filter model, similar to the approach described in [20],

Table II
GENETIC ALGORITHM PARAMETERS

Parameter	Symbol	Value
Initial dummy fitness	f_0	10000
Sharing radius	σ_s	1
Population size	N_P	100
Survival size	- -	75
Mutation rate	- -	0.5
Desired number of species	N_S	10
Seed genotype length	- -	5

where the FIR coefficients are taken to be the impulse response of the Murata MA40S4S transducer. The impulse response model is a 40 kHz sine wave enveloped by a 5th order polynomial, with the coefficients of the polynomial estimated from experimental data. The time series of the impulse response model is shown in Fig. 6, and a comparison between the frequency response of the FIR filter and Murata MA40S4S is shown in Fig. 7.

The simulation used linear chirp signals with alternating sweep direction. The linear chirp pulse is defined by

$$S(t) = \text{rect}\left(\frac{t}{\tau}\right)\sin\left[2\pi\left(\frac{u}{2}t^2 + f_1\right) + \psi\right], \qquad (19)$$

where rect$(\cdot)$ is the rectangular window function, t is the time in seconds, τ is the duration of the pulse in seconds, ψ is the phase in radians/second, and u is given by

$$u = \frac{f_2 - f_1}{\tau}, \qquad (20)$$

where f_1 and f_2 are the starting and ending frequencies of the pulse, respectively. Odd-numbered anchors transmitted linear chirp signals of $f_1 = 38$ kHz and $f_2 = 42$ kHz, while even-numbered anchors transmitted linear chirp signals of $f_1 = 42$ kHz and $f_2 = 38$ kHz. The linear chirp time series was generated using MATLAB's chirp function, and this time series was then padded with zeros equal to the length of the FIR filter impulse response in samples. This zero-padding was necessary to ensure that the entire transmitted signal was simulated, including the transducer's free response after the driving signal has stopped. The final transmitted signal was simulated by passing this zero-padded chirp through MATLAB's filter function, with the coefficients corresponding to the Murata MA40S4S impulse response.

The voltage at the receiver can be estimated by subtracting the total attenuation a_T, calculated using (9), from the MA40S4S's maximum SPL output reference of 120 dB, then taking the antilogarithm and finally multiplying by the original 0 dB reference

$$y_{\text{RMS}} = 10^{(120+a_T)/20}2\times10^{-5} = 2\times10^{1-(a_T/20)}\text{V}_{\text{RMS}}. \qquad (21)$$

B. Simulating Propagation Delay

To simulated propagation delay the distance between the anchor and target is calculated using the the Euclidean distance,

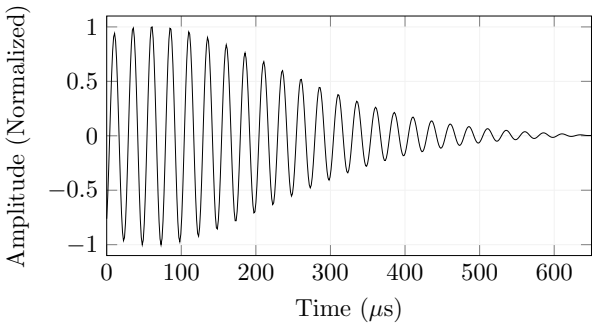

Figure 6. Time series of the FIR model impulse response used to simulate the Murata MA40S4S

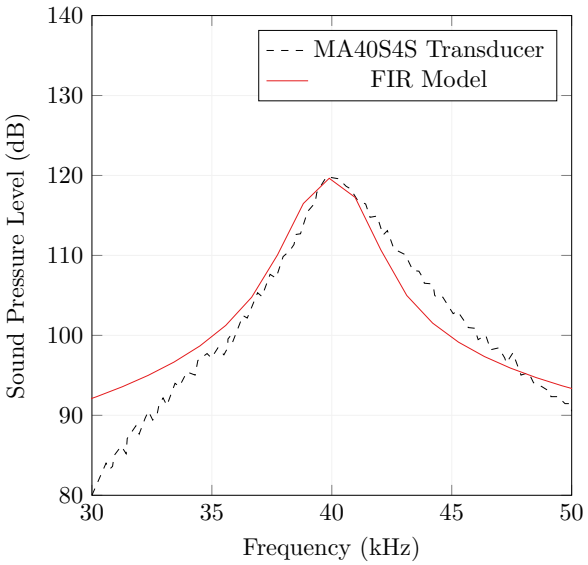

Figure 7. Comparison of the frequency responses of the FIR model (red solid line) and the Murata MA40S4S (black dashed line).

resulting in d_k. The speed of sound is assumed to be a constant $c_0 = 343\ \text{ms}^{-1}$, thus the propagation delay, in samples from the beginning of the frame, is calculated as

$$D_k = N_{0,k} + \text{floor}\left(\frac{d_k}{Tc_0}\right), \qquad (22)$$

where $N_{0,k}$ is the starting sample of the kth time slot and T is the sampling period. The transmitted signal is then inserted into the frame time series at the point D_k, by addition of the transmitted signal, and the existing contents of the time series array. This allows for the effect of fading, as the new pulse will interfere with an pulses that have already been received near D_k.

C. Simulating Reflections & Noise

As previously discussed, the error term ε_k in (1) is affected by multipath reflections. Reflections were simulated as in [4], where each transmitted signal was assumed to be received together with five replicas. Each replica featured a random delay and attenuation with respect to the LOS path. If the received

signal is $y(t)$ then a new signal, containing multipaths, $y_M(t)$ can be generated as

$$y_M(t) = y(t) + \sum_{n=1}^{N_M} g_n y(t - \Delta t_n), \tag{23}$$

where N_M is the number of multipath components, and Δt_n and g_n are the delay and amplitude of the nth multipath component with respect to the LOS Signal. As discussed in [4] this system is sensitive to the selection of g_{max}, that is, the maximum amplitude to which a simulated reflection can be set. In addition, cases of mild and severe multipath can be simulated by adjusting the parameter N_M. In [4] the optimal value of g_{max} was found to be 0.7 and mild multipath was simulated with $g_{max} = 0.7$, $N_M = 1$ whereas severe multipath was simulated with $g_{max} = 0.7$, $N_M = 5$. This work used the later setting for severe multipath to compare the solutions from the GA.

Once all received signals and their reflections were added to the time series, Gaussian noise with a mean of zero and a standard deviation of 0.005 was added to the final signal to simulate environmental background noise.

D. Simulation Method

The simulated UPS used an alternating linear chirp TDMA strategy. The linear chirps used were all 2 ms in duration and with a low frequency of 38 kHz and a high frequency of 42 kHz, odd-numbered anchors swept up from 38 kHz to 42 kHz, whereas even-numbered anchors swept down from 42 kHz to 38 kHz. The simulated sampling rate was selected to be 250000 Samples per second and the time slot duration was 10000 samples. The received time series is processed by cross correlation of each time slot with its respective transmitted signal. The resulting sequence is a quasi-periodic signal, from which the envelope is extracted by applying a Hilbert transform. The maximum of this envelope is used as the arrival time of the signal for the calculation of the time of flight. For position estimation a robust version of the LM algorithm is used [16].

V. Results & Discussion

Results are presented for the optimization with the three different performance objectives. Figs. 8 and 9 present the Pareto frontier for the GDOP metric, Figs. 10 and 11 present the Pareto frontier for WGDOP, Figs. 12 and 13 present the Pareto frontier found using the SLE. The solutions presented in Figs. 9, 11, 13 all achieved 100% target coverage and are presented separately as they are only distinguished by number of anchors and performance metric. When the number of anchors was eight or more, every solution found by the algorithm had 100% target coverage. Examples of anchor layouts found by the optimization using each of the three performance metric are shown in Figs. 18, 19, and 20. Each example shows the solution with the same number of anchors and displays the anchor layout that achieves 100% of room coverage. It is interesting to note that despite small differences in localisation error different optimizations do not converge on similar anchor layout but result in a very different arrangement due to differences in performance metric.

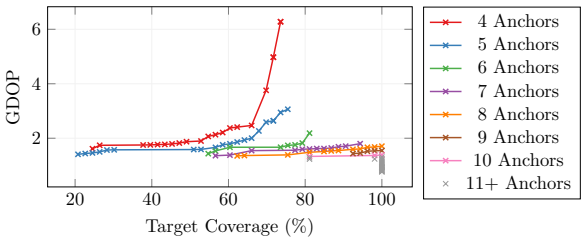

Figure 8. The Pareto frontier for GDOP for solutions with 4 to 10 anchors.

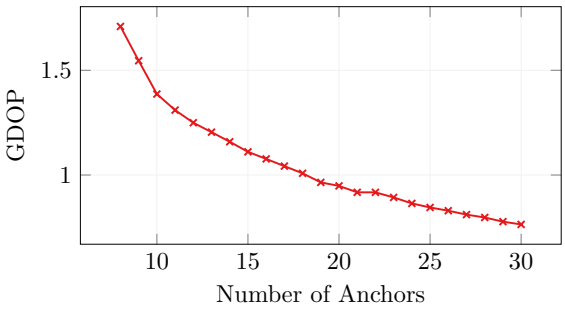

Figure 9. The Pareto frontier for GDOP for solutions with 100% target coverage.

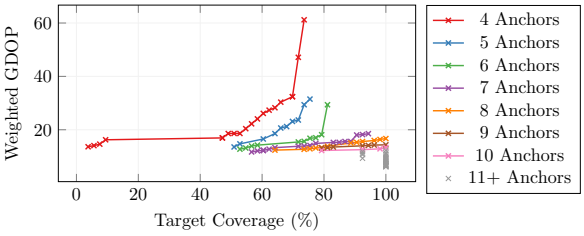

Figure 10. The Pareto frontier for WGDOP for solutions with 4 to 10 anchors.

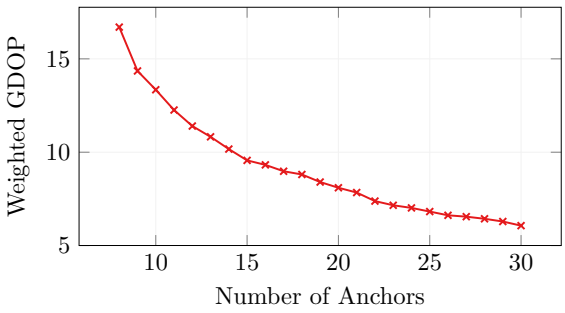

Figure 11. The Pareto frontier for WGDOP for solutions with 100% target coverage.

In Figs. 8, 10, and 12 a clear trade off can be seen between target coverage, localization performance, and number of anchors. Increasing the number of anchors has the effect of increasing both target coverage and localization performance, whereas, for a given number of anchors, increasing the target coverage has a detrimental effect on the localization performance. For this scenario, 100% coverage of all target positions

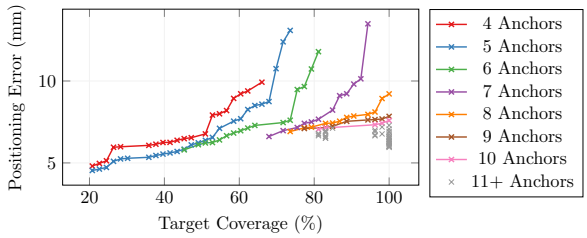

Figure 12. The Pareto frontier for SLE for solutions with 4 to 10 anchors.

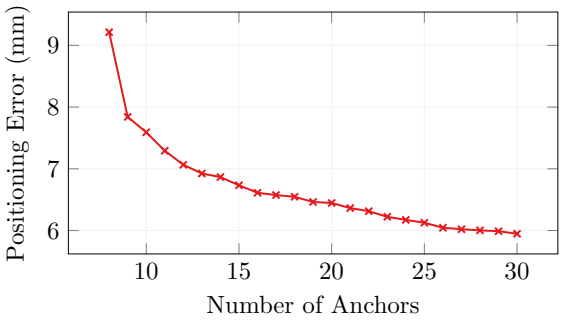

Figure 13. The Pareto frontier for SLE for solutions with 100% target coverage.

is only possible with 9 or more anchors. Figs. 9, 11, and 13 show performance against number of anchors for these 100% solutions for GDOP, WGDOP, and SLE respectively.

As shown in Fig. 12 there is very little performance difference in both target coverage or positioning performance in solutions found using SLE with 7 to 10 anchors. Furthermore, in Fig. 13, it can be seen that increasing the number of anchors from 9 to 19 only decreases the localization error by 2 mm. Presented in Figs. 14, 15, and 16 are the target coverage and positioning error achieved by running the optimal 4 - 10 anchor solutions for GDOP, WGDOP, and SLE through the full time series simulation. Fig. 17 shows the positioning error achieved by all 100% coverage solutions produced by all three objectives.

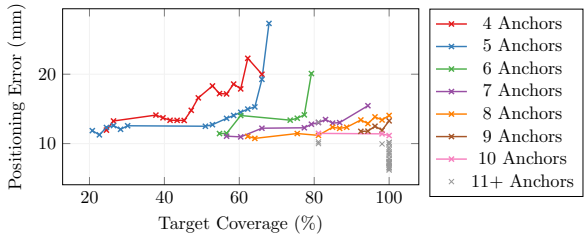

Figure 14. Full time series simulation of GDOP optimum solutions with 4 to 10 anchors.

These figures show that none of the three objectives exactly models the performance of the system, as the objective score plotted in Figs. 14, 15, and 16 no longer meet the criteria for Pareto optimality as defined in (13) and (14). This is unsurprising, as all three performance objectives are simplified models of the true performance of the system. However, this effect becomes less significant as the number of anchors

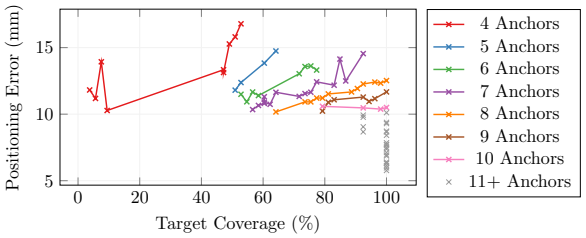

Figure 15. Full time series simulation of WGDOP optimum solutions with 4 to 10 anchors.

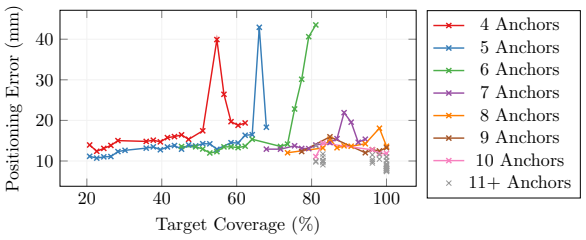

Figure 16. Full time series simulation of SLE optimum solutions with 4 to 10 anchors.

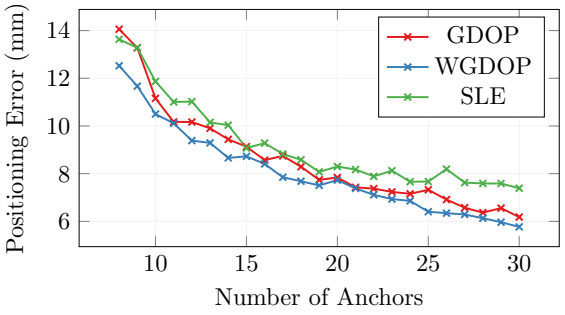

Figure 17. Full time series simulation of all solutions with 100% target coverage.

increases. Such anchor layouts are more resisitve to multipath effects due to having a greater level of reduntency in localizing the target points that they cover. There was no significant difference between the multipath resistance of anchor layouts generated by the three performance metrics.The solutions with low anchors number and high coverage were affected most by multipath.

The worst overall performance is found with the SLE. Despite using the same attenuation and variance model as the WGDOP, the performance is worse. The reduction of performance is due to the random sampling that was applied to generate the noisy range measurements from the variance model in (10). In WGDOP, the value from (10) always the same for a given attenuation, however, in SLE the value from (10) is used to sample a Gaussian distribution. This allows for potentially poor solutions to achieve a good objective score by being randomly assigned less significant range measurement noise. The SLE method also requires more computation than either the GDOP or WGDOP methods, and therefore cannot be recommended as a good objective function.

While the WGDOP objective produces the best overall

results, the difference WGDOP and GDOP solutions is small. It is possible that better solutions could be obtained with WGDOP through further research into more appropriate choices for this model. The model in (10) was obtained from experimental data, and the authors had no better way of determining the model.

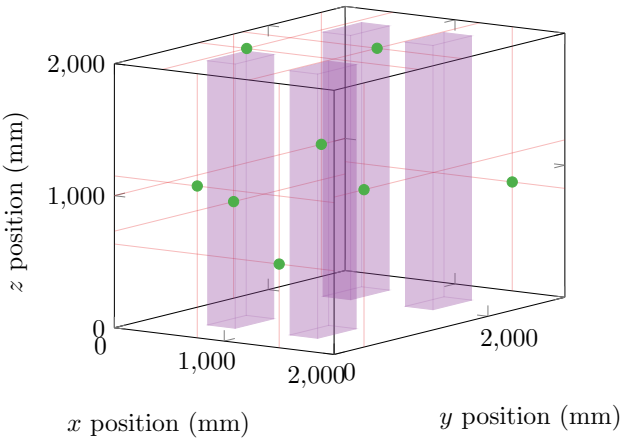

Figure 18. A 9-Anchor, 100% coverage anchor layout found by the optimization using GDOP as a performance metric.

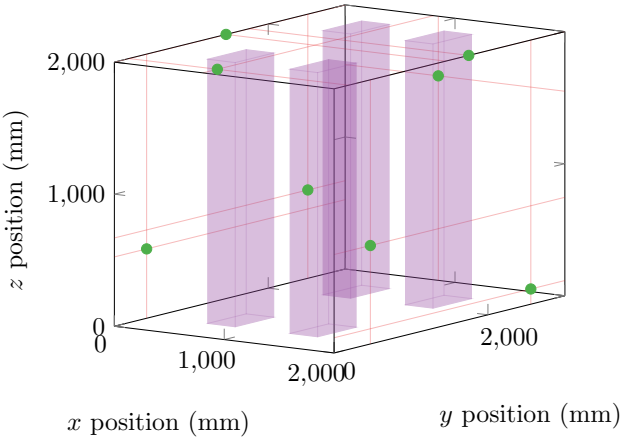

Figure 19. A 9-Anchor, 100% coverage anchor layout found by the optimization using WGDOP as a performance metric.

VI. Conclusion

A comparison of three different performance metrics for anchor position optimization in ultrasonic localization systems has been presented. These metrics were GDOP, WGDOP, and SLE. The optimization was implemented with a multi-objective genetic algorithm based on the NEAT algorithm, with each optimization have three objectives: one of the three performance metrics along with the number of anchors and the percentage of target positions covered by the anchors.

The optimal solutions found by the genetic algorithm were processed by a simulation that used a simulated received time series to localize the target position to obtain a comparison of the three performance metrics. It was found that WGDOP outperformed both the GDOP and the SLE methods, although

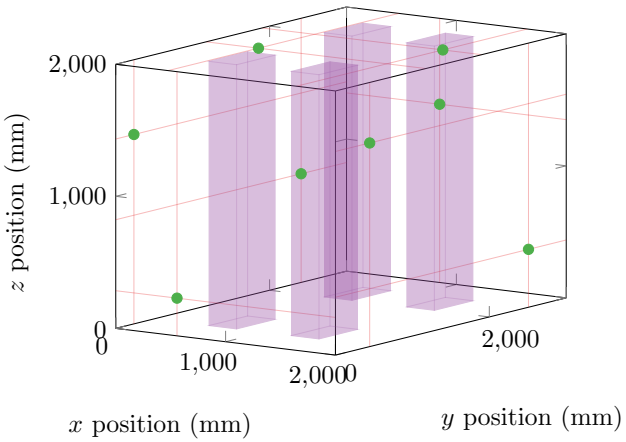

Figure 20. A 9-Anchor, 100% coverage anchor layout found by the optimization using SLE as a performance metric.

the difference in performance is small. The worst performance overall was in solutions generated using the SLE performance metric, and this was due to the effects of random sampling that was used to assess fitness using this objective. The computation of SLE is considerably more expensive than either GDOP or WGDOP due to the need for multiple applications of the LM algorithm in estimating position. WGDOP only requires a small increase in the number of quantities that must be computed, and it results in increased performance over GDOP by including additional information that affects position estimation.

References

[1] J. Urena, A. Hernandez, J. J. Garcia, J. M. Villadangos, M. Carmen Perez, D. Gualda, F. J. Alvarez, and T. Aguilera, "Acoustic Local Positioning With Encoded Emission Beacons," *Proceedings of the IEEE*, vol. 106, no. 6, pp. 1042–1062, Jun. 2018.

[2] R. Yarlagadda, I. Ali, N. Al-Dhahir, and J. Hershey, "GPS GDOP Metric," *IEE Proceedings - Radar, Sonar and Navigation*, vol. 147, no. 5, pp. 259–264, 2000.

[3] M. Iqbal, M. Naeem, A. Anpalagan, A. Ahmed, and M. Azam, "Wireless sensor network optimization: Multi-objective paradigm," *Sensors (Switzerland)*, vol. 15, no. 7, pp. 17 572–17 620, 2015.

[4] A. Comuniello, A. Moschitta, and A. De Angelis, "Ultrasound TDoA Positioning Using the Best Linear Unbiased Estimator and Efficient Anchor Placement," *IEEE Transactions on Instrumentation and Measurement*, vol. 69, no. 5, pp. 2477–2486, 2020.

[5] J. O. Roa, A. R. Jiménez, F. Seco, J. C. Prieto, and J. Ealo, "Optimal Placement of Sensors for Trilateration: Regular Lattices vs Meta-heuristic Solutions," in *Computer Aided Systems Theory – EUROCAST 2007*, 2007, pp. 780–787.

[6] F. Domingo-Perez, J. L. Lazaro-Galilea, I. Bravo, A. Gardel, and D. Rodriguez, "Optimization of the coverage and accuracy of an indoor positioning system with a variable number of sensors," *Sensors (Switzerland)*, vol. 16, no. 6, 2016.

[7] C. S. Chen, "Weighted geometric dilution of precision calculations with matrix multiplication," *Sensors (Switzerland)*, vol. 15, no. 1, pp. 803–817, 2015.

[8] N. Kirchhof, "Optimal placement of multiple sensors for localization applications," in *2013 International Conference on Indoor Positioning and Indoor Navigation, IPIN 2013*, no. October, 2013, pp. 28–31.

[9] J. O'Rourke, *Art gallery theorems and algorithms*, J. E. Hopcroft, G. D. Plotkin, J. T. Schwartz, D. S. Scott, and J. Vuillemin, Eds. New York, NY, USA: Oxford University Press, 1987.

[10] M. Laguna, J. O. Roa, A. R. Jimenez, and F. Seco, "Diversified local search for the optimal layout of beacons in an indoor positioning system," *IIE Transactions (Institute of Industrial Engineers)*, vol. 41, no. 3, pp. 247–259, 2007.

[11] S. B. Chaudhry, V. C. Hung, R. K. Guha, and K. O. Stanley, "Pareto-based evolutionary computational approach for wireless sensor placement," *Engineering Applications of Artificial Intelligence*, vol. 24, no. 3, pp. 409–425, 2011.
[12] K. O. Stanley and R. Miikkulainen, "Evolving neural networks through augmenting topologies," *Evolutionary Computation*, vol. 10, no. 2, pp. 99–127, 2002.
[13] K. O. Stanley and R. Miikkulainen, "Competitive coevolution through evolutionary complexification," *Journal of Artificial Intelligence Research*, vol. 21, pp. 63–100, 2004.
[14] N. Levanon, "Lowest GDOP in 2-D scenarios," *IEE Proceedings: Radar, Sonar and Navigation*, vol. 147, no. 3, pp. 149–155, 2000.
[15] S. Haigh, J. Kulon, A. Partlow, P. Rogers, and C. Gibson, "A Robust Algorithm for Classification and Rejection of NLOS Signals in Narrowband Ultrasonic Localization Systems," *IEEE Transactions on Instrumentation and Measurement*, vol. 68, no. 3, pp. 646–655, Mar 2019.
[16] S. Haigh, J. Kulon, A. Partlow, P. Rogers, and C. Gibson, "Improved Obstacle Mitigation and Localization Accuracy in Narrowband Ultrasonic Localization Systems Using RoBCUL Algorithm," *IEEE Transactions on Instrumentation and Measurement*, vol. 69, no. 5, pp. 2315–2324, May 2020.
[17] M. J. Crocker, *Handbook of acoustics*. New York, NY, USA: Wiley, 1998.
[18] A. Comuniello, G. D. Angelis, A. D. Angelis, and A. Moschitta, "Effect of transducer directivity on ultrasound 2D positioning system accuracy," in *2018 IEEE International Systems Engineering Symposium (ISSE)*. Rome, Italy: IEEE, Oct 2018, pp. 1–6.
[19] K. Deb, A. Pratap, S. Agarwal, and T. Meyarivan, "A fast and elitist multiobjective genetic algorithm: NSGA-II," *IEEE Transactions on Evolutionary Computation*, vol. 6, no. 2, pp. 182–197, 2002.
[20] S. Murano, C. Perez-Rubio, D. Gualda, F. J. Alvarez, T. Aguilera, and C. D. Marziani, "Evaluation of Zadoff–Chu, Kasami, and Chirp-Based Encoding Schemes for Acoustic Local Positioning Systems," *IEEE Transactions on Instrumentation and Measurement*, vol. 69, no. 8, pp. 5356–5368, Aug 2020.